

Thermal Modelling of Gypsum Plasterboard Assemblies Exposed to Standard Fire Tests

D. Lázaro^{1*}, E. Puente¹, M. Lázaro¹, P. G. Lázaro¹, J. Peña²

¹GIDAI, University of Cantabria, Avda. Los Castros, s/n, 39005 Santander. SPAIN

²GRUPO URALITA, División Yesos Ibéricos, Ctra de Andalucía Km. 30,200, 28340 Madrid SPAIN

ABSTRACT

Gypsum plasterboards are widely used for compartmentation and for retarding the spread of fire in buildings. Although numerous heat transfer studies have been conducted, literature indicates there are extensive differences in the thermal properties used in these studies. Comprehensive experimental and numerical analyses have been conducted to elucidate the leading factor in the ablation of a gypsum board system when it is exposed to the standard fire resistance test.

A methodology based on both simultaneous thermal analysis and computational modelling is proposed to understand the behaviour of a gypsum plasterboard when the boundary temperature increases quickly as one side of the wall is subjected to the standard ISO 834.

Finally, four different wall assemblies made of a commercial fireproof plasterboard system are exposed to the standard test. The temperature on the unexposed face is examined to validate the computational model of the plasterboard.

KEYWORDS: heat transfer, compartment fires, fire modelling, fire resistance tests, gypsum plasterboards, thermogravimetric analysis.

1. INTRODUCTION

Gypsum plasterboards are widely used as passive fire protection elements because of their superior fire resistance and relatively inexpensive production costs. There are two main types of gypsum plasterboards; Type A corresponds to the conventional gypsum plasterboard, and Type F (or Type X) refers to ‘fire-resistant’ gypsum plasterboard. Gypsum plasterboard consists of a porous gypsum core between two layers of paper, creating a sandwich structure. These gypsum plasterboards can be assembled on different systems regardless of the use of insulated material between the plasterboards or the use of one or multiple layers of gypsum plasterboard. Although they have been widely studied, there are still many discrepancies [1] in the values of the thermal properties and the related modelling of heat transfer behaviour.

The values of thermal conductivity and specific heat, and the methods used to determine these thermal properties are the most controversial. Some studies determine conductivity by analysing the gypsum across the different temperature steady states that it undergoes during degradation processes. These studies include the analysis of the conductivity before and after dehydration and the analysis of the gypsum subjected to the ISO 834 curve up to 1000°C [2, 3]. Additionally, because gypsum is porous, most studies convert convection, pore radiation, and ablation into equivalent thermal conductivity to determine transient conductivity [4, 5].

Further discrepancies arise from the complexity of modelling chemical reactions undergone by gypsum in fire. Gypsum dihydrate ($\text{CaSO}_4 \cdot 2\text{H}_2\text{O}$) crystals theoretically contain 21% of water by weight [6]. This water is primarily lost during two consecutive and temperature-overlapped dehydration processes that gypsum undergoes at atmospheric pressure between 80 °C and 250°C.



Sultan et al. [7] and Pérez-Moreno et al. [8] determined the second dehydration process occurring at a temperature of approximately 600°C. However, the most common approach is to consider the two dehydration processes over the previously mentioned temperature range. Our results also fit this value in the typical range. Considering our results and those of Sultan et al., it can be presumed that the second dehydration process is masked by the large peaks in specific heat due to the first decomposition reaction from gypsum to the hemihydrates [9]. Using a pinhole lid increases the water content in the gas phase over the degradation zone of the sample, which makes the second dehydration more difficult (i.e., the required temperature is shifted to a higher value). Thus, the overlap between dehydration reactions [10] is changed.

Once chemical water is lost, the plasterboard can reabsorb water; however, there is a third endothermic reaction in the gypsum at approximately 360°C. This reaction induces a transition between a material (sol) that is easy to rehydrate by forming hemihydrates and another material (insol) that is difficult to rehydrate by absorbing water (because it has a different crystalline structure) [11, 12].



Here, Q is the energy released in the reaction.

Conventionally, more reactions occurring in gypsum at higher temperatures can be distinguished; however, they may be related to the decomposition (or thermal oxidation) of impurities contained within the gypsum. To identify the reactions that occur in gypsum at higher temperatures, we must analyse the impurities (i.e. by X-ray diffraction) because different reactions may occur at the same temperature depending on the type of impurities [13, 14, 15].

However, we ignore the effects of impurities on the thermal behaviour of gypsum plasterboard because the reactions that affect the impurities occur at temperatures over 500°C. Our simulations consider that ablation will begin with the third endothermic reaction (around 360°C).

Once the values of the parameters that characterize the behaviour of gypsum were determined by small-scale tests, we employed four standard tests to validate the results for a large-scale model [16, 17, 18]. The standards define tests for the different non-load-bearing elements such as walls and ceilings. In the present study, we examined four tests with different configurations (two cladding walls and two partition walls).

The objective of the standard fire tests is to evaluate the fire resistance behaviour of a building system under well-defined boundary conditions of temperature and pressure [16]. According to EN 1363-1, a linear pressure gradient exists along the height of the furnace. Although the gradient will vary slightly as a function of the furnace temperature, a mean value of 8.5 Pa per meter height may be assumed in assessing the furnace pressure conditions. These tests enable us to quantify the capacity of the system to bear high temperatures and, thus, provide information regarding the behaviour of gypsum assemblies under fire conditions.

2. SMALL-SCALE TESTS

As mentioned previously, we developed small-scale tests to determine thermal properties: specific heat by simultaneous thermal analysis (STA)—Netzsch STA 449 F3—and thermal conductivity analysis by laser flash apparatus (LFA) using a pulse light technique—Netzsch LFA 447. In addition, these tests were performed to elucidate the thermodynamic characteristics of the thermal processes occurring in the gypsum plasterboard core during heating.

First, a detailed thermal analysis of two different gypsum-plasterboard samples was conducted (Table 1). The tests were performed in an air atmosphere at a heating rate of 10°C/min. The temperatures range was 30–800°C. All tests were performed without the pan lid.

Thermogravimetric parameters, such as the residue and extrapolated onset temperature (T_{onset}) [19], were directly obtained from the STA tests. The onset temperature corresponds to the temperature at which the loss of mass begins.

- Sample 1 (type A, 12.89 mg): Residue = 0.81 and $T_{\text{onset}} = 80^\circ\text{C}$
- Sample 2 (type F, 19.77 mg): Residue = 0.80 and $T_{\text{onset}} = 80^\circ\text{C}$

Figure 1 shows the STA (heat flow and mass loss) results for both samples. Note that there is only one peak in the range between 80°C and 180°C (at approximately 150°C) that we attribute to dehydration reactions working as competitive reactions (meaning that the onset temperature of the second process occurs before the endset temperature of the first process). The presence of just one peak is attributable to the open pan configuration, which avoids the accumulation of saturated water vapour and the absorption of water on the surface of the sample, thus rehydrating a portion of this sample. In these reactions, the gypsum plasterboard lost approximately 16% mass, which is the amount contained within as chemical water. Once these processes occur, the gypsum becomes a soluble anhydride of CaSO_4 . The third reaction, which occurs at approximately 358 °C in sample 1 and at 360°C in sample 2, is a reaction related to a transition in the crystalline structure from the soluble to the insoluble anhydride CaSO_4 . This steady state of gypsum did not overlap with any other reaction and the sample mass remained constant. At this point, the material cannot absorb a significant amount of water. Furthermore, when gypsum does not have any chemical water, it becomes brittle (less resistance and flexibility).

The remaining processes are associated with the type and amount of impurities and additives in the gypsum. However, in the present study, these reactions are not considered because we assume that the gypsum board mechanically breaks down before achieving the reaction temperatures of the impurities (after 500 °C).

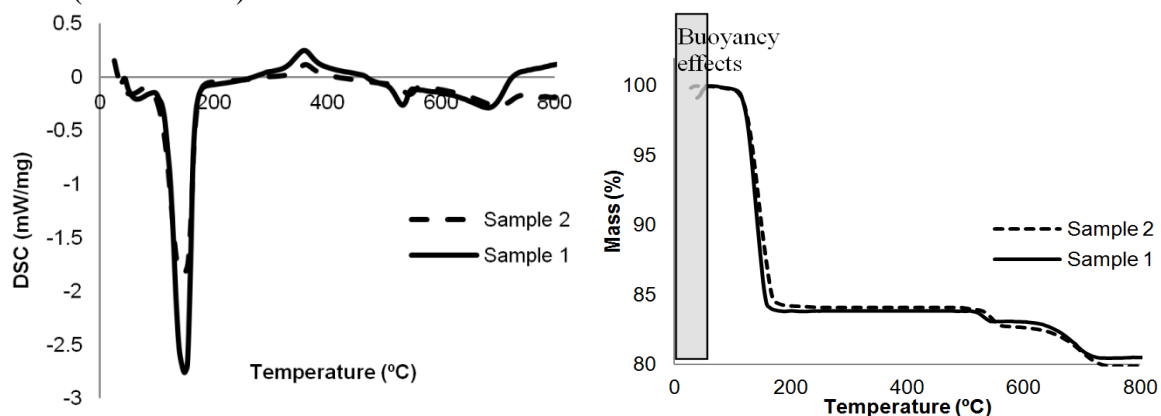


Fig. 1. STA analysis of gypsum plasterboards.

For the gypsum plasterboard, we determined the effective specific heat by using sapphire ($\alpha\text{-Al}_2\text{O}_3$) as the reference material. Three tests were performed in the STA: one without a sample, another with the reference sample, and the last with the material under investigation. It is important to note that buoyancy effects did not let us accurately correct the mass loss curve [20], and thus all the derivative properties obtained from mass loss. Finally, the effective specific heat was calculated using ASTM E1269 [21]:

$$C_p(T) = \frac{HF_{sample} - HF_{blank}}{HF_{ref} - HF_{blank}} \times \frac{Mass_{ref}}{Mass_{sample}} \times C_{pref}(T) \quad (4)$$

Here, HF is the heat flow (kW) obtained from STA and C_{pref} is the specific heat of sapphire in the same temperature range.

Figure 2 shows the effective specific heat values for the range of temperatures in the test. The effective specific heat comprises the sum of the actual specific heat of the gypsum plasterboard, the thermal effects of the dehydration reaction, and the third reaction [22]. The negative specific heat values observed in the test results are related to the exothermic character of the third reaction. The manufacturer indicates that, in order to achieve the actual specific heat, it is necessary to avoid the ranges of temperatures where reactions take place. Measuring the effective specific heat allow us to include the necessary energy for dehydration in the specific heat curve into the computational model.

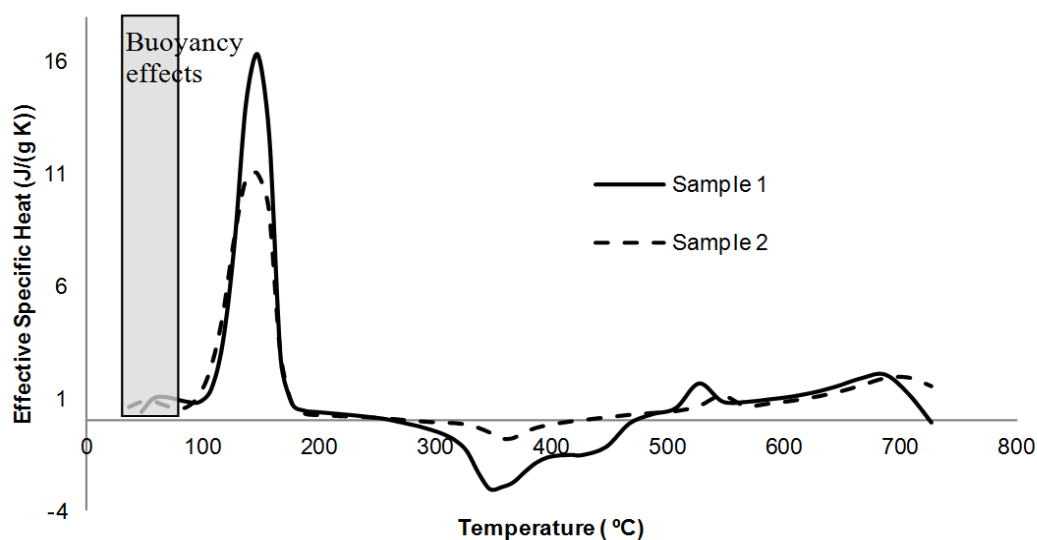


Fig. 2. Effective specific heat of the gypsum samples.

The thermal diffusivity of the samples was obtained in the range of 30–250°C (Figure 3). The technique was introduced by Parker et al. [23] and represents both a direct method for measuring the thermal diffusivity and an indirect method for measuring the thermal conductivity the material when thermal expansion and specific heat are known.

The Cape-Lehman model [24], which considers radial heat loss from the unexposed face, was employed to determine thermal diffusivity by using the relationship between the sample thickness (d in meters) and the time at which the temperature of the unexposed face reaches half of the maximum value ($t_{1/2}$ in seconds) [23].

$$\alpha = 0.1337 \frac{d^2}{t_{1/2}} \quad (5)$$

Density was obtained using the mass-temperature curve from thermogravimetric analysis, considering a constant volume of material (Figure 4). This assumption of constant volume is supported by the low linear expansion coefficient of the gypsum plasterboard (approximately $15 \times 10^{-6} \text{ }^\circ\text{C}^{-1}$ [25]). This value assumes an increase in thickness of:

$$\Delta L = L_0 \cdot (e^{\alpha \cdot \Delta T} - 1) \quad (6)$$

Over the range of 250 $^\circ\text{C}$ tested in the LFA, the thickness increases by 0.37%.

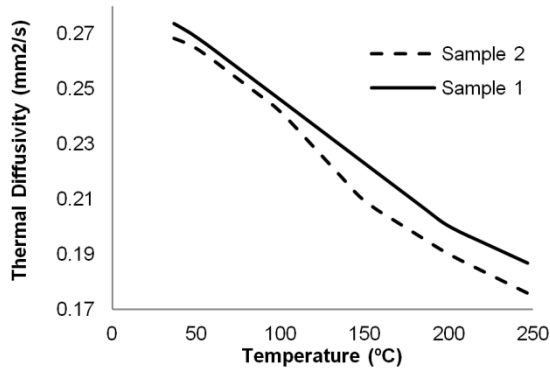


Fig. 3. Thermal diffusivity from LFA analysis.

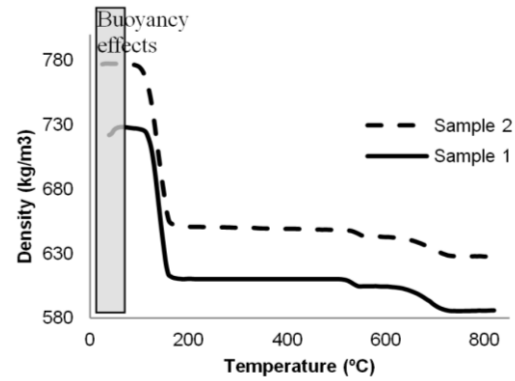


Fig. 4. Density calculated for the gypsum samples.

Regarding conductivity, studies listed in the bibliography reflect the same behavioural tendency. However, other studies were performed by drying the samples; therefore, they do not consider water content [26] or they studied gypsum conductivity in a steady state [2]. In the present study, we obtained the thermal conductivity considering the actual specific heat and the measured thermal diffusivity. The actual specific heat does not consider the dehydration enthalpy.

To determine the conductivity of the gypsum board (Figure 5), we used the following relation of thermal diffusivity:

$$\alpha = \frac{k}{\rho \cdot c_p} \quad (7)$$

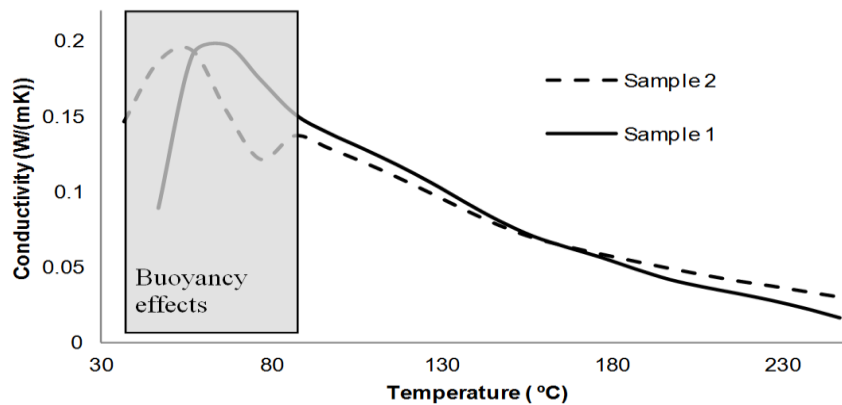


Fig. 5. Conductivity calculated for the gypsum samples.

3. STANDARD FIRE TESTS

The European normative standards EN 1363 and EN 1364 [16-18] established the requirements to perform fire resistance tests for non-load-bearing elements, walls, and ceilings. The test furnace must maintain the average temperatures specified by the standards (Figure 6).

$$T = 345 \cdot \log_{10}(8t + 1) + 20 \quad (8)$$

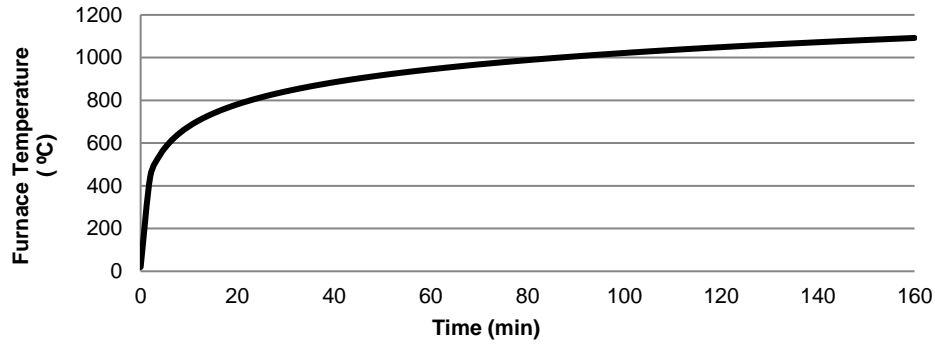


Fig. 6. Normalized temperature at the furnace.

There are two criteria in the standards for failure of the test:

- The average temperature of the unexposed face increases to more than 140°C over the initial temperature.
- The temperature at any point of the unexposed face increases to more than 180°C over the initial temperature.

In the present study, we analysed the results of four fire resistance tests, including different wall systems based on gypsum plasterboards, while considering two types of gypsum. The characteristics of these samples are listed in Table 2. Test 1 consisted of two pairs of commercially available 12.5 mm Type A gypsum plasterboards, separated by an air gap of 46 mm and joined by C-shaped steel studs. Test 2 consisted of a cladding wall composed of a pair of commercially available 12.5 mm Type A gypsum plasterboards, also joined by C-shaped steel studs. Test 3 consisted of two pairs of commercially available 15 mm Type F gypsum plasterboards separated by an air gap of 92 mm and joined by two C-shaped steel studs. Test 4 consisted of a cladding wall composed of four commercially available 15 mm Type F gypsum plasterboards.

Figure 7 shows the distribution of the temperature measurement points. The wall of the figure has a height of 3 m and a width of 3 m. C and F denote the temperatures on the unexposed face of the system; A and D are the thermocouples on the interior face of the exposed board; and B and E are points located on the interior face of the unexposed boards. The number of temperature measurements designated with the symbols 'CT' refer to the unexposed board temperature obtained with the thermographic camera.

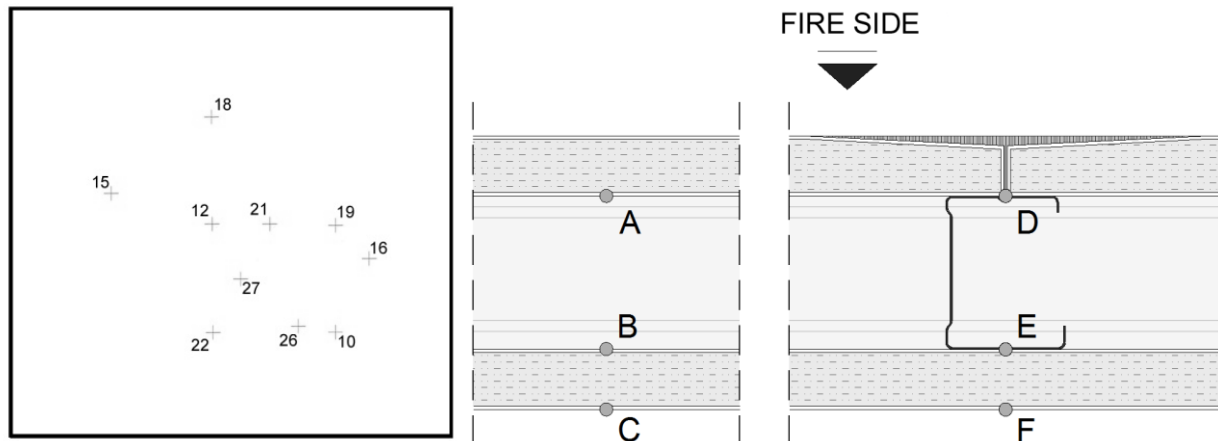


Fig. 7. Temperature points on the wall (left). In depth plane without (centre) and with studs (right).

Figure 8 shows the temperatures measured in depth at points 12 (without stud) and 21 (with stud) during Test 1. In Tests 2 to 4 we obtained only the temperature on the unexposed face (Figures 9, 10, and 11). Our numerical approach needs to be validated against these temperatures to verify the credibility of the test results.

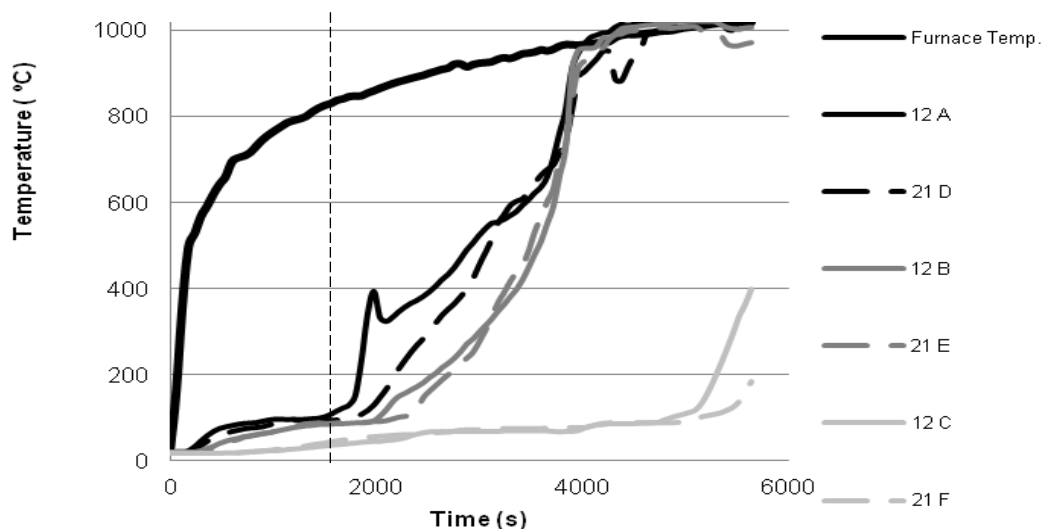


Fig. 8. Test 1: Temperatures of the different layers of the solution.

As shown, temperatures at A and B (as well as those at D and E) of the wall system are very close during the first stages of the test. However, the difference between them grew gradually when the furnace temperature exceeded 800°C (dashed vertical line in Figure 10). At this time, the temperature at A (and D) begins to grow from approximately 100°C, while that of B (and E) seems to be steady for slightly longer.

At this moment, the exposed board (system of boards) is almost dehydrated, whereas dehydration is just beginning on the unexposed board. The temperatures at A and B (and those at D and E) did not increase at the same time because radiation is the primary factor. The delay in time taken for a difference in temperature between A and D (B and E) to occur is due to the high level of heat dissipation of steel compared to gypsum.

Once the first board falls off, there is a sudden increase in the temperature of the unexposed face. This may be because of the combined effect of ablation and consequent convection of hot air into the

air gap and radiation heat transfer through both the hole and the porous media of gypsum at high temperatures. We do not know the exact time when the exposed board fell but we can determine by observation that this time was between 3720 s and 4000 s for test 1 and between 6900 s and 7140 s for test 3. We do not have time data from the cladding walls tests.

If we monitor the ‘failure point’ (the point where the temperature limit was reached), the tendency of the temperatures in the rear face was similar in all tests. Stages varied owing to the number of plasterboards, but the stabilization stage and increase in the final temperature were the same because of the combined effects of ablation and radiation. In the last stages of the resistance test, radiation through the pores became the primary factor leading to the ‘failure point’. This is because at high temperatures, water migrates from the pores and radiation through the pores becomes significant (since it is proportional to temperature to the power of three), which highly improves the heat transfer [27].

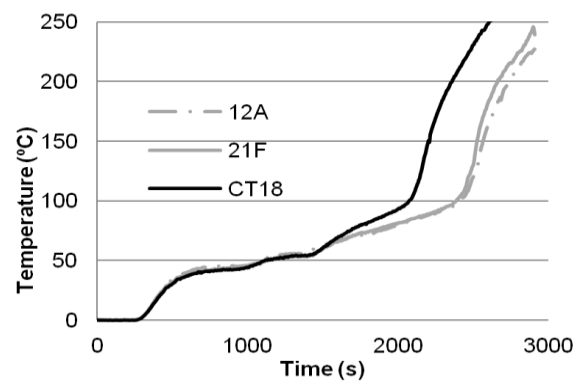


Fig. 9. Test 2: Temperature of the unexposed surfaces

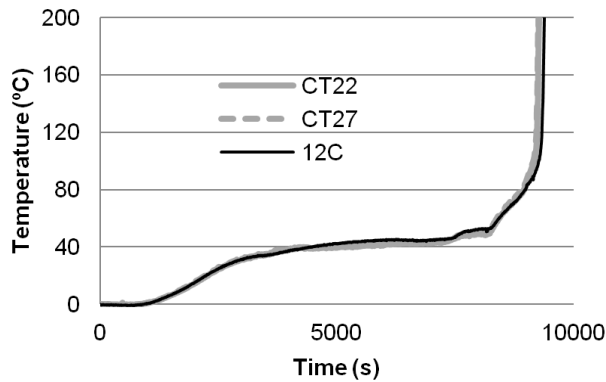


Fig. 10. Test 3: Temperature of the unexposed surfaces.

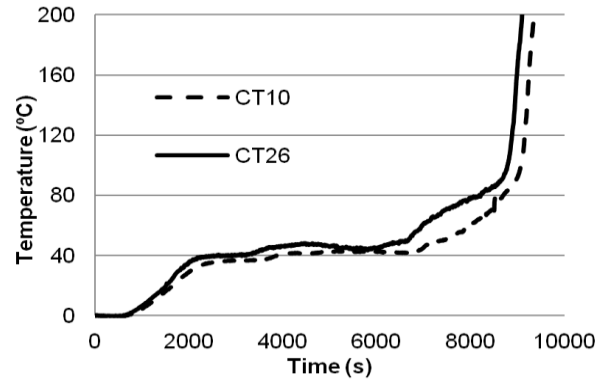


Fig. 11. Test 4: Temperature of the unexposed surfaces.

Figures 12 to 15 show the temperature distribution on the rear faces. This distribution of temperatures was measured using a thermographic camera during the entire test (FLIR SC 640, focal length 19.31 mm). These figures show the maximum temperature obtained on the unexposed face, the zones at which the fault occurs first, and the fissures that appear in the board.

Furthermore, we use thermographic data to predict the exact instant and position of the system failure because in the resistance tests, the thermocouples are in fixed positions. The failure occurs when the temperature in these positions reaches 180°C at a point or the average temperature reaches 140°C over the initial temperature. We use this temperature data from the unexposed side for validation purposes.

In all the tests, the boards were fixed to the oven structure on the top, bottom, and left sides. On the right side, an insulation material (ceramic wool) was used to avoid holes, which could enable heat

loss from the interior of the oven. The steel structure must be taken into consideration when analysing the cladding walls. Furthermore, the element for monitoring the deformation was at the same position (on the right side) in all the tests except for test 4, where it is, more or less, at the centre line.

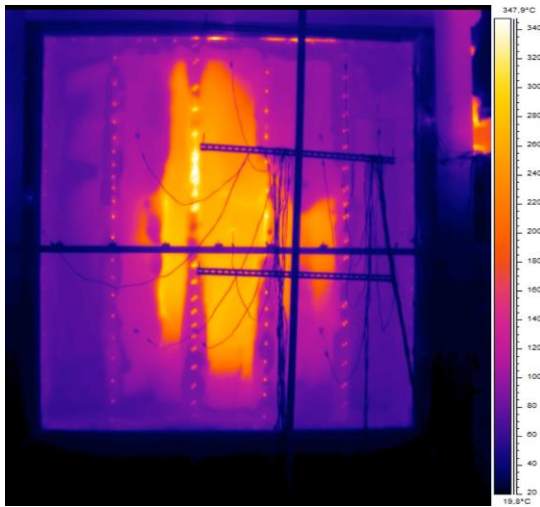


Fig. 12. Test 1: Temperature distribution at 95 min [19.8-347.9°C]

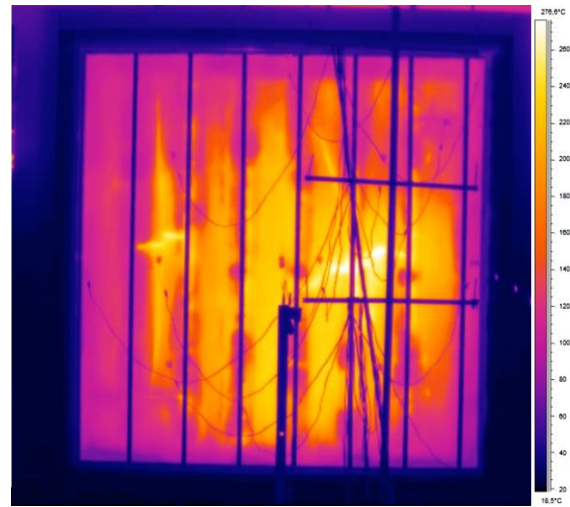


Fig. 13. Test 2: Temperature distribution at 45 min [18.5-376.6°C].

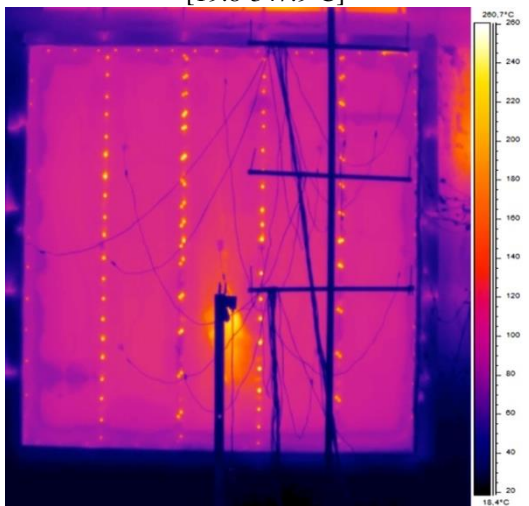


Fig. 14. Test 3: Temperature distribution at 155 min [18.4-260.7°C].



Fig. 15. Test 4: Temperature distribution at 165 min [19.3-312.4°C].

Figures 12-15 show the high temperature reached by the screws. In addition, it is notable that, in most of the tests, temperature (average or maximum) is responsible for the failure of the system but not for the deformation. If we divide the plasterboard into nine equal areas (AR01, AR02, ..., AR09), as in Figure 16, we can obtain the temperature distribution over the unexposed board at the moment of the test failure. Table 3 shows the average and maximum temperatures for any element of the layout.

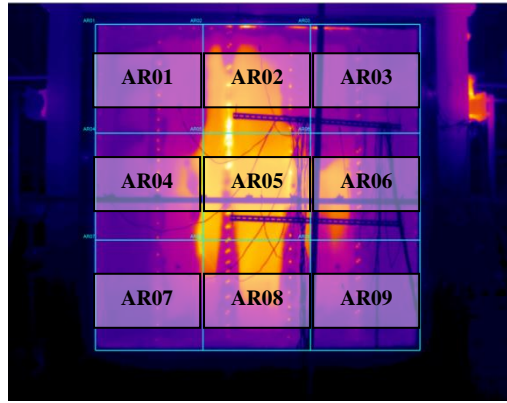


Fig. 16. Layout of temperature areas.

The maximum temperatures were observed to be slightly higher than the maximum values allowed by EN 1363. This is because the thermocouples did not register the maximum temperature zone, and in the last steps of the heat transfer through the boards, the temperature curve increased sharply.

Despite the differences between all the tests, both maximum and average temperatures at the central column, comprised of the AR02, AR05, and AR08 areas, is higher than the lateral columns. In addition, AR05 achieved the maximum temperatures both at the peak and at the average. However, the central row (AR04, AR05, and AR06) was not clearly different because the steel structure between the camera and the board interfered with the monitoring.

Tests 1 and 3 (partition elements) show that the average temperature of the top elements (AR01, AR02, and AR03) is higher than those of the bottom ones (AR07, AR08, and AR09) in test 1, but not in test 3. However, tests 2 and 4 (cladding walls) showed that the bottom elements are hotter than the top ones.

Finally, Figures 17 and 18 show some of the gypsum plasterboard assemblies after the tests. The remaining gypsum boards were dehydrated and brittle. They also had a lower solubility and their mechanical resistance was practically zero.



Fig. 17. Cracking system failure.

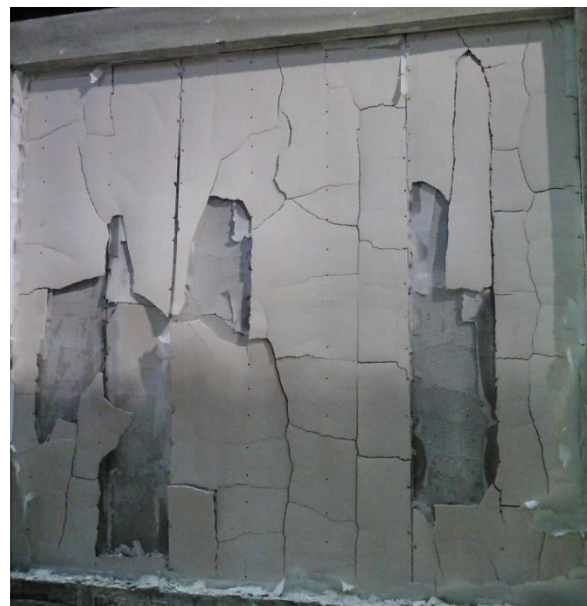


Fig. 18. System after the test.

4. MODELLING APPROACH

In this study, the numerical model was developed using the Fire Dynamics Simulator (FDS) [28], considering the parameters determined experimentally in the small-scale tests. STA provided the specific heat and, for a given reaction, the relative amounts of products (i.e. water), the reference temperature at which the reaction takes place, and the temperature range of the reaction. In our numerical approach, we simply considered the global dehydration reaction with a maximum rate at the peak of the STA enthalpy record. We also prescribed the pyrolysis range of temperatures from the onset temperature to the endset temperature. Mass loss along the global dehydration reaction was directly obtained from the STA mass loss record.

The model considers a gypsum sample of $50 \times 50 \text{ mm}^2$, with a mesh size of 5 mm for the gas zone and 2.5 mm for solids. The reported 2.5 mm size is the mean size of the dedicated computational mesh used by FDS to solve the 1D heat conduction equation. It is possible because the solid regions obeyed the ‘one cell thick’ rule of FDS. We use CELL_SIZE_FACTOR=0.5 to decrease the mesh size from 5 mm to 2.5 mm. We set the required temperature on the exposed face. This temperature follows the European normative standards EN 1363 and EN 1364 [16-18]. When applying boundary conditions to the back side, the model considers the attribute BACKING=‘EXPOSED’. This attribute is used when FDS is required to calculate the heat transfer through the solid into the space behind the solid. The wall emissivity of all gypsum plasterboards is assumed to equal 0.88. We set the heat transfer coefficient to be $8 \text{ W/m}^2 \text{ } ^\circ\text{C}$ at the exposed and unexposed surfaces.

The model was set to predict the ablation of the gypsum board by employing approaches related to the ablation behaviour undergone by the gypsum board at elevated temperatures. Ablation cracks were modelled by setting the temperature of the back of the boards where an equivalent mass of gypsum of $10 \times 10 \text{ mm}^2$ was removed from the simulation. We consider the hypothesis that the temperature at which ablation and shrinkage cracks appear was related to the peak temperature of the third reaction. Subsequently, the internal structure of the gypsum changes, becoming a brittle powder. This method can be performed for any type of gypsum by directly using the STA results.

Figure 19 shows the temperature distribution inside exposed boards of Test 3 simulation. Isotherms 80, 150, and 180 define the dehydrated region at any time during the test. Isotherm 360 corresponds in this case to the temperature that defines the ablation. This is the temperature of the sample 2 third reaction (Figure 1). Therefore, in the figure, we see how this temperature is approximated on the unexposed side through the plasterboard, and when it reaches this side, the model assumes that the plasterboard fell off.

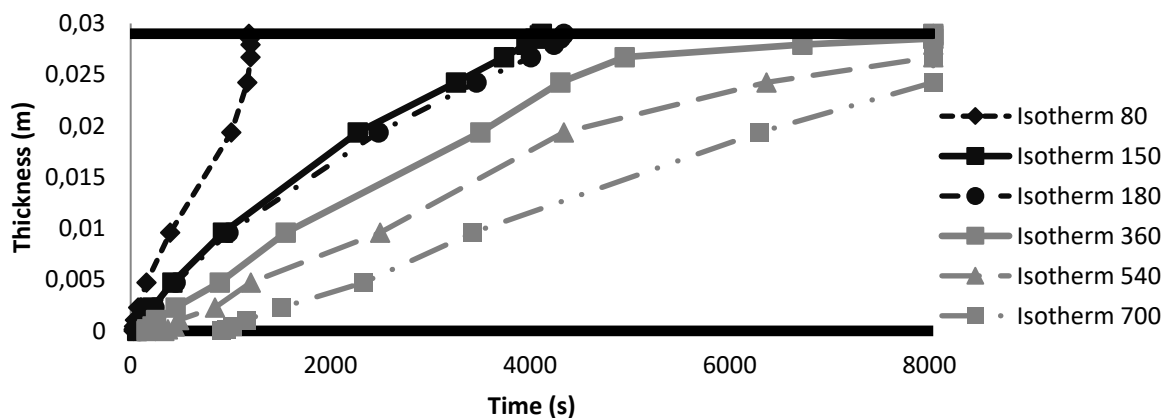


Fig. 19. Numerical temperature profiles inside plasterboard for Test 3.

Simplified curves of conductivity and specific heat were inputted to the computer model. Figure 20 compares these conductivities with some of the values obtained from past studies [4, 5, 29, 7, 30, 31, 32], without considering the dehydration process. As shown, to improve the evaluation of heat transfer between solid obstructions by FDS, some assumptions were made for the thermal conductivity in each wall assembly. Case 1 refers to the ceiling and cladding walls and Case 2 to the partition solution. XB means that system has a number X of boards. Additionally, some approaches included systems composed of more than one board in contact with each other. The bigger a building system, the lower is its conductivity coefficient. This approach considers the contact interface between layers that obstruct heat transfer. We have used similar trends to those reported in the papers listed in the bibliography.

At high temperatures, water migrates from the pores and the radiation through the pores becomes significant, which greatly improves the heat transfer. The heat transfer through the gypsum pores was modelled by convection and radiation. To consider this, we assume an increase in the thermal conductivity of gypsum at temperatures above 800°C. This equivalent conductivity allows accelerated radiation in voids at high temperatures [33]. We add this equivalent conductivity to the calculated conductivity with the measured specific heat and thermal diffusion.

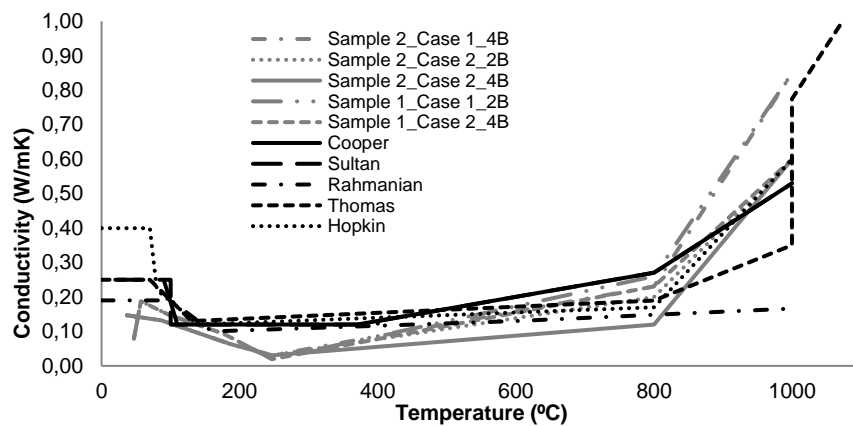


Fig. 20. Comparison of thermal conductivity values of gypsum with the reference values.

Equation 7 was used until 250°C. After this temperature, we define two tables with thermal conductivity values. These thermal conductivities depend on the number of boards and on the configuration (Table 4). Thermal conductivities are adjusted with the validation of the computer model against the experimental results. The more tests we use for validation, the more accurate is the adjustment.

The effective specific heat (Figure 21) arises from the necessity of simulating different phases of gypsum. We consider some of the most relevant points of the effective specific heat measured with the STA (Figure 2) and introduce those values into FDS. We also remove negative values that are not associated with a mass loss. We keep the previous values from the third reaction.

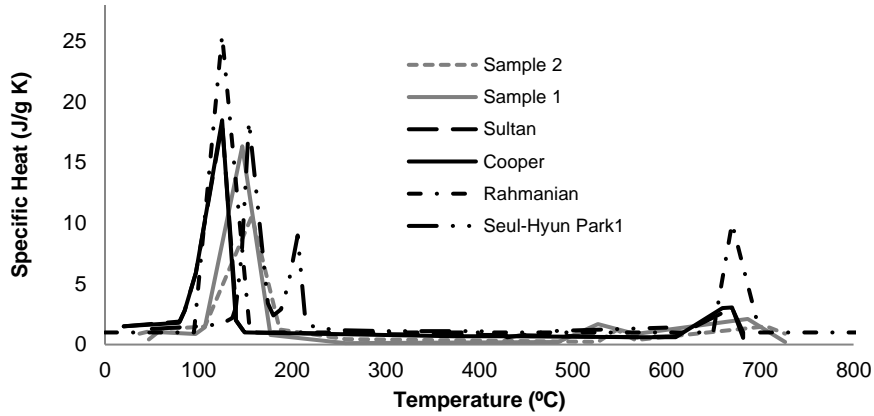


Fig. 21. Comparison of specific heat values of gypsum with the reference values.

Finally, to validate the numerical model of the gypsum plasterboard reactions, we compared the model results against several standard fire tests, as described in the following section.

5. VALIDATION OF THE MODEL

Figures 22 and 25 show the comparisons between the temperature measurements of the unexposed boards from the standard tests and the model under investigation. In general, the time of system failure is accurately predicted. Better approximations are achieved for the partition solutions (Tests 1 and 3), in which the model predicts the temperature increase before system failure. These models account for the ablation of the exposed faces by considering the previously described hypothesis. However, for cladding wall solutions, the model fails to capture the shape of the temperature increase.

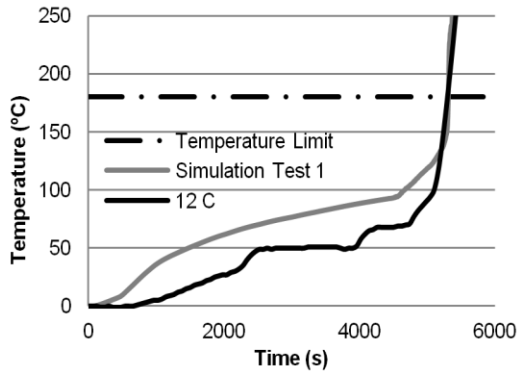


Fig. 22. Validation of the computational model for Test 1.

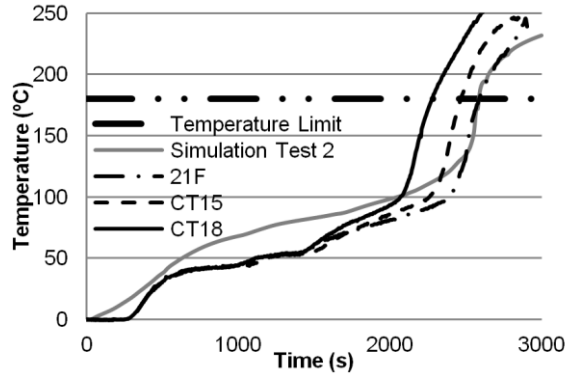


Fig. 23. Validation of the computational model for Test 2.

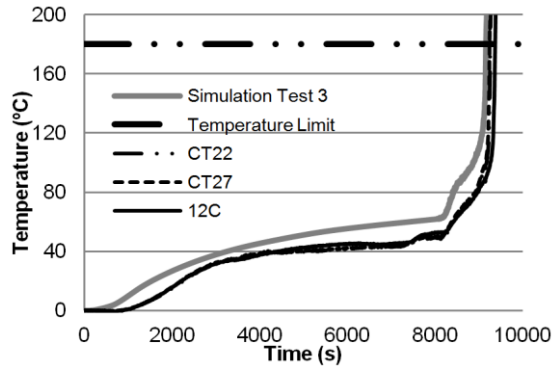


Fig. 24. Validation of the computational model for Test 3.

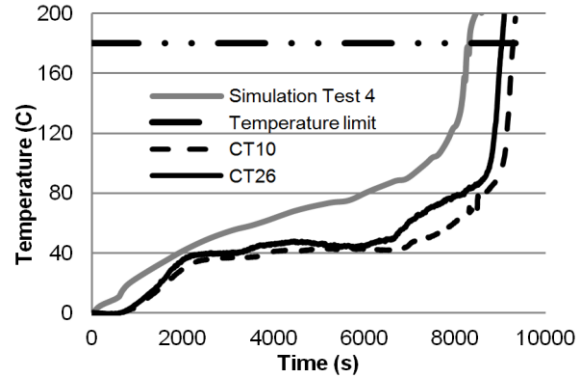


Fig. 25. Validation of the computational model for Test 4.

Table 5 lists the dispersion between the model and the experimental temperature values. The absolute and relative errors were calculated at certain relevant times.

Cladding wall model simulations have the worst approximation to the real test. This is because our model has been validated using the hypothesis of the ablation at the temperature of the third reaction, and this fact is the most relevant factor in the system failure of the partition configurations. In the case of cladding walls, the failure is determined only by the conductivity of the boards. In this case, we should consider the drawback that the FDS model has to simulate conductivity through parallel obstructions. Our model, as for the models used in studies described in the literature, does not consider the presence of cardboard on the boards during the simulation.

In the fire resistant test simulation, the most important parameter is the failure time. According to this parameter, the errors are less than 13.6% even for the worst case.

6. CONCLUSIONS

This paper presents the results of four fire resistance tests. These results include valuable time-temperature data for the different configurations and the novelty of recorder temperature results obtained by a thermographic camera. The thermographic camera was able to collect real-time points of system failure even if they did not correspond with the locations of the thermocouples. Therefore, it was possible to record the distribution of temperature on the unexposed side. These results facilitate a better validation of thermal transfer models because they consider the fast heat transfer zone.

At elevated temperatures (around 360 °C), there is a third endothermic reaction in the gypsum that implies a transition between a material that is easy to rehydrate by forming hemihydrates and another material that is difficult to rehydrate by absorbing water. A new hypothesis has been developed to consider the ablation in the model for the exposed boards of the partition systems; this hypothesis considers the temperature of the third endothermic reaction as the ablation temperature.

The characterization procedure performed in this study estimated the global behaviour of different types of board against standard tests satisfactorily. The model quickly predicted the time at which the system failed by considering the thermal properties of the gypsum in use. However, to predict the temperatures in systems with multiple layers, it is necessary to adapt the thermal conductivity at high temperatures according to the construction solution under consideration. This is because of the limitations present in determining certain thermal properties, such as the conductivity between the interfaces of the plasterboards. Figure 25 shows that the cladding wall configuration with four boards

provides the worst approximation of the temperature. Thus, the thermal conductivity is adapted by basing it on the construction system to be modelled.

REFERENCES

- [1] Korte, A. C. J., Brouwers, H. J. H. Calculation of thermal conductivity of gypsum plasterboards at ambient and elevated temperature, *Fire Mater.* 2010; 34: 55–75
- [2] Wullschleger, L., Wakili, K. G. Numerical parameter study of the thermal behaviour of a gypsum plaster board at fire temperatures, *Fire Mater.* 2008; 32: 103–119
- [3] ISO 834-8:2002 Fire-resistance tests -- Elements of building construction -- Part 8: Specific requirements for non-loadbearing vertical separating elements
- [4] Rahmanian, I., Wang, Y. Thermal Conductivity of Gypsum at High Temperatures A Combined Experimental and Numerical Approach, *Acta Polytechnica*, 2009: 49 (1): 16-20
- [5] Thomas, G. Thermal Properties of Gypsum Plasterboard at High Temperatures, *Fire Mater.* 2002; 26: 37–45 (DOI: 10.1002/fam.786)
- [6] Mehaffey, J. R., Cuerrier, p. and Carisse, G. A. 1994. A model for predicting heat transfer through gypsum-board/wood-stud walls exposed to fire. *fire and materials*, 18, 297-305]
- [7] Sultan, M. A. A model for predicting heat transfer through non-insulated unloaded steel-stud gypsum board wall assemblies exposed to fire, *Fire Technology*, 1996: 32 (3): 239-259
- [8] Pérez-Moreno, S. M., Gazquez, M. J., Barneto, A. G., Bolivar, J. P. Thermal characterization of new fire-insulating materials from industrial inorganic TiO₂ wastes, *Thermochimica Acta* 2013: 552 114– 122
- [9] Wakili, K. G., Hugi, E., Wullschleger, L., Frank, T. H. Gypsum board in fire modelling and experimental validation. *Journal of Fire Sciences* 2007; 25(3):267–282.
- [10] Lou, W., Guan, B., Wu, Z. Dehydration behavior of FGD gypsum by simultaneous TG and DSC analysis, *J Therm Anal Calorim* 2011: 104:661–669
- [11] Manzello, S. L., Gann, R. G., Kukuck S. R., Lenhert, D. B., Influence of gypsum board type (X or C) on real fire performance of partition assemblies, *Fire Mater.* 2007; 31:425–442
- [12] Melinge, Y., Lanos, C., Nguyen, K. S., Daiguebonne, C., Guillou, O., Freslon, S., One-Dimensional-Time Study of the Dehydration of Plasterboards Under Standard Fire Condition (ISO 834): Thermo-Chemical Analysis, *Journal of fire sciences*, 2011, 29 - 4: 299-316
- [13] Yu, Q. L., Brouwers, H. J. H. Thermal properties and microstructure of gypsum board and its dehydration products: A theoretical and experimental investigation, *Fire Mater.* 2012; 36: 575–589
- [14] Kolarkar, P., Mahendran, M. Experimental studies of gypsum plasterboards and composite panels under fire conditions, *Fire Mater.* 2012: 38 (1): 13–35
- [15] Ghazi Wakili K, Hugi E. Four types of gypsum plaster boards and their thermo-physical properties under fire condition. *Journal of Fire Sciences* 2009, 27(1), 27-43.
- [16] EN 1363-1: Fire Resistance Tests. Part 1: General Requirements. 1999
- [17] EN 1364-1: Fire Resistance Tests for Non-Loadbearing Elements - Part 1: Walls, 1999
- [18] EN 1364-2: Fire Resistance Tests for Non-Loadbearing Elements - Part 2: Ceilings, 1999
- [19] ISO 11358. Thermogravimetry (TG) of polymers. General principles, 1997.

- [20] Speyer, R., Thermal Analysis of Materials, Taylor & Francis, 1993, ISBN 9780824789633, page 116 of 298
- [21] ASTM E1269, Standard Method for Determining Specific Heat Capacity by Differential Scanning Calorimetry, ASTM International, (2005) West Conshohocken, USA.
- [22] D. I. Kolaitis, M. A. Founti, Development of a solid reaction kinetics gypsum dehydration model appropriate for CFD simulation of gypsum plasterboard wall assemblies exposed to fire, *Fire Safety Journal* 58 (2013) 151–159
- [23] Parker, W.J., Jenkins, R.J., Butler, C.P., Abbott, G.L. Method of Determining Thermal Diffusivity, Heat Capacity and Thermal Conductivity, *Journal of Applied Physics* 32 (9): 1679. doi:10.1063/1.1728417
- [24] Cape, J. A., Lehman, G. W. Temperature and Finite Pulse-Time Effects in the Flash Method for Measuring Thermal Diffusivity, *J. Appl. Phys.* 34, i 7, 1909 (1963)
- [25] Sistemas Constructivos con Placa de Yeso Laminado, ATEDY, Asociación técnica y empresarial del yeso, page 14 of 160. (<http://www.atedyplacayeso.com/compendio.pdf>)
- [26] Benichou, N., Sultan, M. A. Thermal properties of lightweight-framed construction components at elevated temperatures, *Fire Mater.* 2005; 29:165–179
- [27] M.A. Othuman, Y.C. Wang, Elevated-temperature thermal properties of lightweight foamed concrete, *Construction and Building Materials* 25 (2011) 705–716
- [28] Floyd, J., Forney, G., Hostikka, S., Korhonen, T., McDermott, R., McGrattan, K. Fire Dynamics Simulator (Version 6) – User’s Guide. National Institute of Standards and Technology (NIST). December 2012
- [29] Hopkin, D. J., Lennon, T., El-Rimawi, J., Silberschmidt, V. V. A numerical study of gypsum plasterboard behaviour under standard and natural fire conditions, *Fire Mater.* 2012; 36:107–126
- [30] Cooper, L. Y. The Thermal Response of Gypsum-Panel / Steel-Stud Wall Systems Exposed to Fire Environments – A Simulation for Use in Zone-Type Fire Models, NISTIR 6027, Building and Fire Research Laboratory, National Institute of Standards and Technology, Gaithersburg, Maryland, June 1997.
- [31] Chu Nguong, N. Calcination of Gypsum Plasterboard under Fire Exposure, *Fire Engineering Research Report* 04/6 May 2004
- [32] Park, S., Manzello, S. L., Bentz, D. P., Mizukami, T. Determining thermal properties of gypsum board at elevated temperatures, *Fire Mater.* (2009) DOI: 10.1002/fam
- [33] D.A. Kontogeorgos, M.A. Founti A generalized methodology for the definition of reactive porous materials physical properties: Prediction of gypsum board properties, *Construction and Building Materials* 48 (2013) 804–813

TABLES

Table 1. Basic properties of two samples in the study

	NORMATIVE	DENSITY		MASS
	UNE EN 520	Theoretical (kg/m ³)	Sample (kg/m ³)	Sample (mg)
Sample 1	A	724	722	12.891
Sample 2	F	766	777	19.769

Table 2. Assemblies of the gypsum boards tested under European normatives EN 1363 and EN 1364

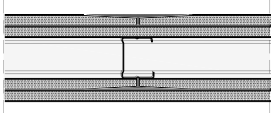

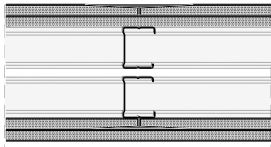
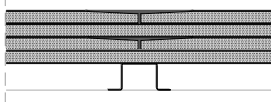
Test	Ambient Temperature (°C)	Building system	Gypsum	Configuration
1	20		Sample 1	Partition
2	22		Sample 1	Cladding walls
3	22		Sample 2	Partition
4	23		Sample 2	Cladding walls

Table 3. Temperature layout.

test 1			test 2		test 3		test 4	
Label	Max (°C)	Avg (°C)	Max (°C)	Avg (°C)	Max (°C)	Avg (°C)	Max (°C)	Avg (°C)
AR01	215.1	89.1	226.2	116.6	341.0	101.0	196.4	92.4
AR02	384.8	170.4	232.5	139.3	290.9	104.0	213.6	91.8
AR03	337.9	79.3	211.2	109.2	240.2	90.0	259.3	103.0
AR04	303.1	105.8	262.1	148.2	297.7	107.7	254.1	122.6
AR05	390.5	223.1	284.4	194.6	379.4	117.6	313.4	135.6
AR06	250.6	100.8	282.4	159.8	283.6	96.7	310.5	163.5
AR07	288.2	83.0	222.3	120.2	298.2	97.0	265.7	109.5
AR08	282.5	135.5	243.8	152.5	355.9	114.8	314.8	129.1
AR09	212.0	75.0	239.0	113.6	238.9	92.1	318.2	138.2

Table 4. Thermal conductivity values over 250 °C

Cladding walls			
Number of boards	800°C		1000°C
	Sample 1	Sample 2	Samples 1 and 2
1	0.3	0.3	1
2	0.26	0.25	0.85
3	0.24	0.23	0.85
4	0.24	0.23	0.85

Partition			
Number of boards	800°C		1000°C
	Sample 1	Sample 2	Samples 1 and 2
2	0.2	0.2	0.6
4 or more	0.23	0.12	0.6

Table 5. Simulation errors

	t1 (s)	t2 (s)	t3 (s)	t4 (s)	t5 (s)	t6 (s)		Time of system collapse
Test 1	2520	3900	4260	4740	5100	5340	Test 1	
Temperature_exp (°C)	49	50	68	71	100	204	Time_exp (s)	5340
Temperature_sim (°C)	61	68	70	95	113	245	Time_Sim (s)	5270
Relative error (%)	23.75	35.88	2.28	33.48	13.42	20.07	Relative error (%)	1.31
Absolute error (°C)	-12	-18	-2	-24	-13	-41	Absolute error (s)	70
Test 2	650	1450	2050	2280	-	-	Test 2	
Temperature_exp (°C)	39	56	97	180	-	-	Time_exp (s)	2280
Temperature_sim (°C)	52	82	100	115			Time_Sim (s)	2590
Relative error (%)	32.16	45.74	3.17	-37.86	-	-	Relative error (%)	13.60
Absolute error (°C)	-13	-26	-3	65	-	-	Absolute error (s)	-310
Test 3	3000	7550	8920	9250	-	-	Test 3	
Temperature_exp (°C)	33	48	80	189	-	-	Time_exp (s)	9250
Temperature_sim (°C)	38	61	103	242			Time_Sim (s)	9165
Relative error (%)	16.19	26.41	28.73	27.80	-	-	Relative error (%)	0.92
Absolute error (°C)	-5	-13	-23	-53	-	-	Absolute error (s)	85
Test 4	2370	6715	8660	9045	-	-	Test 4	
Temperature_exp (°C)	39	103	91	180	-	-	Time_exp (s)	9045
Temperature_sim (°C)	58	154	327	332			Time_Sim (s)	8330
Relative error (%)	49.22	98.14	261.02	84.32	-	-	Relative error (%)	7.9
Absolute error (°C)	-19	-51	-236	-152	-	-	Absolute error (s)	715